ELSEVIER

International Journal of Heat and Fluid Flow 22 (2001) 417–423

International Journal of HEAT AND FLUID FLOW

www.elsevier.com/locate/ijhff

Analysis of the swirl effect on turbulent length scales in an ICE cylinder by two-point LDV

H. Belmabrouk [a,*], M. Michard [b]

[a] Faculté des Sciences de Monastir, Département de Physique, Boulevard de L'Environnement, Monastir 5000, Tunisia

[b] Laboratoire de Mécanique des Fluides et d'Acoustique, ECL, UCB-Lyon1, CNRS UMR 5509, Ecole Centrale de Lyon, BP 163, 69131 Ecully, France

Received 30 October 1999; accepted 23 December 2000

Abstract

Two-point laser Doppler velocimetry is used to investigate the turbulent flow behind an axisymmetric cylinder head simulating the intake stroke of an internal combustion engine. Profiles of axial, radial and tangential mean and RMS velocities as well as profiles of integral length scales are measured at several distances from the cylinder head. The effect of non-homogeneity of the flow on integral length scale is investigated. The effects of swirl and valve lift on integral scales are also analysed. The temporal spectra of the tangential fluctuating velocity are measured to identify the swirl centre precession.

Keywords: Laser Doppler velocimetry; Turbulence scales; Swirling flows; Internal combustion engines; Spectral analysis

1. Introduction

Combustion processes and heat transfer in reciprocating engines depend strongly on the turbulent characteristics of the flow inside the cylinder. The understanding of the basic mechanisms such as flame–turbulence interaction, as well as their numerical modelling, requires a detailed description of the turbulent field. In particular, it is necessary to provide information about the time and length scales of the turbulent motion (Lance et al., 1991). These scales are related to some physical mechanisms, for instance, integral length scales provide a measure of the energy-containing eddies. Due to the non-homogeneity and unsteadiness of the in-cylinder flow, the experimental determination of turbulence length scales proves to be difficult. Many techniques have been proposed in the literature to measure the time or the space correlation coefficients from which the turbulent length scales can be deduced indirectly assuming the validity of the Taylor hypothesis or directly (Belmabrouk and Michard, 1998). These techniques are based either on hot-wire anemometry or laser Doppler velocimetry. The conditions required for the application of the Taylor hypothesis are unlikely to be satisfied in engines. Therefore, the techniques based on the space correlation coefficient are more accurate.

The method used in this paper is based on two-colour dual-beam laser Doppler velocimetry. By measuring simultaneously the turbulent velocity in two different points separated by a variable distance, it is possible to obtain the space correlation coefficient and the integral and Taylor length scales. The aim of this paper is to characterise the turbulent flow in a steady flow rig behind an axisymmetric cylinder head simulating the induction stroke of a motored engine.

In the following section, we recall the definitions of the correlation coefficient and the integral length scale. Then, the measuring technique, the experimental set-up and the operating conditions are presented. To characterise the basic features of the mean flow, profiles of mean and RMS velocities and integral length scales are presented. The effect of non-homogeneity on the symmetry of the correlation coefficient curve and on the integral length scale is then investigated. Finally, the effect of swirl on integral scales is analysed and the temporal spectra are measured in order to characterise the swirl-centre precession.

2. Theoretical background

2.1. Correlation coefficient

Let $u_i(\boldsymbol{x},t)$ be the ith component of the fluctuating velocity at position $\boldsymbol{x}$ and time t in a Cartesian frame with unit vectors $(\boldsymbol{e}_1,\boldsymbol{e}_2,\boldsymbol{e}_3)$. The space correlation coefficient of this component measured simultaneously at positions $\boldsymbol{x}$ and $\boldsymbol{x}+r\boldsymbol{e}_j$ is defined according to

$$R_{ii}^{(j)}(r,\boldsymbol{x}) = \frac{\overline{u_i(\boldsymbol{x},t)\,u_i(\boldsymbol{x}+r\boldsymbol{e}_j,t)}}{\sqrt{\overline{u_i^2(\boldsymbol{x},t)}}\sqrt{\overline{u_i^2(\boldsymbol{x}+r\boldsymbol{e}_j,t)}}}. \quad (1)$$

It is worth noting that the tensor summation is not being used here. The double subscript i refers to the velocity component

* Corresponding author. Tel.: +216-3-500-274; fax: +216-3-500-278.
E-mail address: hafedh.belmabrouk@fsm.rnu.tn (H. Belmabrouk).

0142-727X/01/$ - see front matter
PII: S0142-727X(01)00075-3

whereas the superscript j stands for the direction of the moving probe displacement. The vector $\boldsymbol{x}$ represents the position of the fixed probe and r is the distance, along the jth axis, between the fixed and moving probes.

The bar in Eq. (1) stands for the time averaging operator.

2.2. Integral length scale

The integral length scale corresponding to $R_{ii}^{(j)}(r,\boldsymbol{x})$ is defined by

$$L_{ii}^{(j)}(\boldsymbol{x}) = \int_0^{\infty} R_{ii}^{(j)}(r,\boldsymbol{x})\,\mathrm{d}r. \tag{2}$$

Since the integral length scale is deduced from the correlation using an integration, this scale is weakly sensitive to experimental errors as well as to the probe size. The effect of these parameters on the integral length scale was investigated experimentally by Belmabrouk (1992) and theoretically by Belmabrouk (2001).

3. Measuring technique and experimental set-up

3.1. Two-point laser Doppler velocimetry

The method used here is based on laser Doppler velocimetry. A two-colour dual-beam system is used to generate two measuring volumes. One is kept fixed, while the other can be moved by use of an optical device. A detailed description of the measuring techniques is available in Belmabrouk and Michard (1998). Some features of the technique are given hereafter. A beam expander, with an expansion ratio of 1.94, is used to reduce the size of the probe volume. Two photomultipliers operating in the forward scattering mode detect the scattered light from seeding particles crossing each probe. The signals are processed by two Dantec 55L96 counters. As simultaneous measurements of the velocity at the two points are required to calculate the correlation coefficient, a Dantec 57G149 coincidence detector with an adjustable acceptance window width is used.

An achromatic lens (focal length = 310 mm, diameter = 80 mm) is used to focus the four laser beams in order to create two different probe volumes. The beam separation on the focusing lens is 42.5 mm. The spatial separation r between the probes is adjusted using two mirrors forming a dihedron with an adjustable angle. One mirror remains fixed while the other can be rotated. The moving mirror is equipped with two micrometric screws that can activate the moving probe, either vertically, or in a direction parallel to the optical axis of the laser. The resolution of the displacement of the distance between the probes is about 0.03 mm for a focal length of 310 mm.

3.2. Experimental set-up

A general view of the steady flow assembly is presented in Fig. 1. The rig comprises a centrifugal fan, a flow smoothing section including honeycombs and filters, and a cylindrical test section (diameter $D = 120$ mm, length = 500 mm). The cylinder head adopted for this study is described in Belmabrouk et al. (1991). A single central valve is used in order to produce a nearly axisymmetric mean flow. The valve head diameter is 40 mm and the valve seat angle is 45°. The valve lift is kept fixed to obtain a steady flow. The removable swirl generator involves four inclined blades and is located upstream of the valve. More detailed sketches of the valve and its seat are available in Belmabrouk et al. (1991). The air flow is usually maintained fixed at 196 m^3/h, which corresponds to a flow rate per unit surface or a mean velocity $U_d = 5$ m/s or a Reynolds number $Re = (U_d D)/\nu = 4 \times 10^4$.

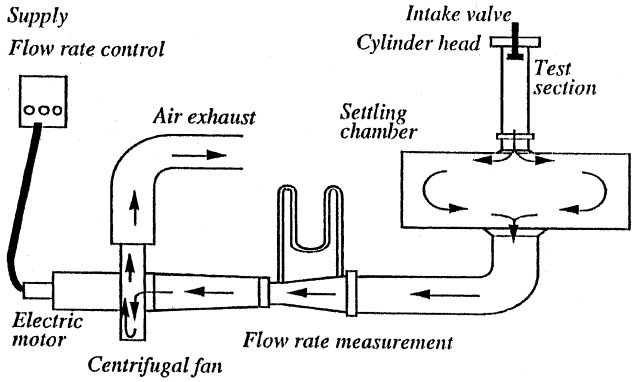

Fig. 1. Steady flow assembly.

Table 1
Designation of co-ordinate directions and velocity components

Velocity component	V (radial)	W (tangential)	U (axial)
Direction	1	2	3
Co-ordinate	X	ϕ (not used)	Z

The origin O of the co-ordinate frame is located at the intersection of the cylinder axis and the plane of the cylinder head. The Z-axis, denoted by subscript 3, corresponds to the axis of the cylinder and it is pointed down. The radial direction is denoted by X or subscript 1. Table 1 summarises the subscripts used to designate co-ordinate directions and velocity components.

4. Results and discussion

4.1. Basic features of the mean flow

The turbulent flow inside the cylinder is defined, in the first step, by the profiles of axial and tangential mean and RMS velocities at different sections, valve lifts and flow rates. The statistics are performed by ensemble averaging over a large set of uncorrelated measurements. The sample of the profiles presented here corresponds to a valve lift $L_v = 10$ mm and a flow rate per unit surface or a mean velocity $U_d = 5$ m/s. The selected sections are situated at $Z/D = 0.17$, 0.58, 1.21 and 2.17 from the cylinder head.

4.1.1. Without swirl

Fig. 2(a) shows the profiles of the axial mean velocity $\overline{U}$ normalised by U_d versus the radial distance X scaled by the cylinder diameter $D = 120$ mm when the flow rig is not fitted with the swirl generator. The flow in the upper part of the cylinder is characterised by three zones: the intake jet that exhibits large axial velocities, the recirculation zone behind the valve with negative velocity and a relatively homogeneous distribution of the RMS velocity, and the vortex in the corner between the side wall and the cylinder head. The test section $Z/D = 0.58$ is located downstream of the impinging of the valve jet on the side wall and the recirculation zone becomes larger. In the section $Z/D = 2.17$, the flow is uniform except in boundary layers.

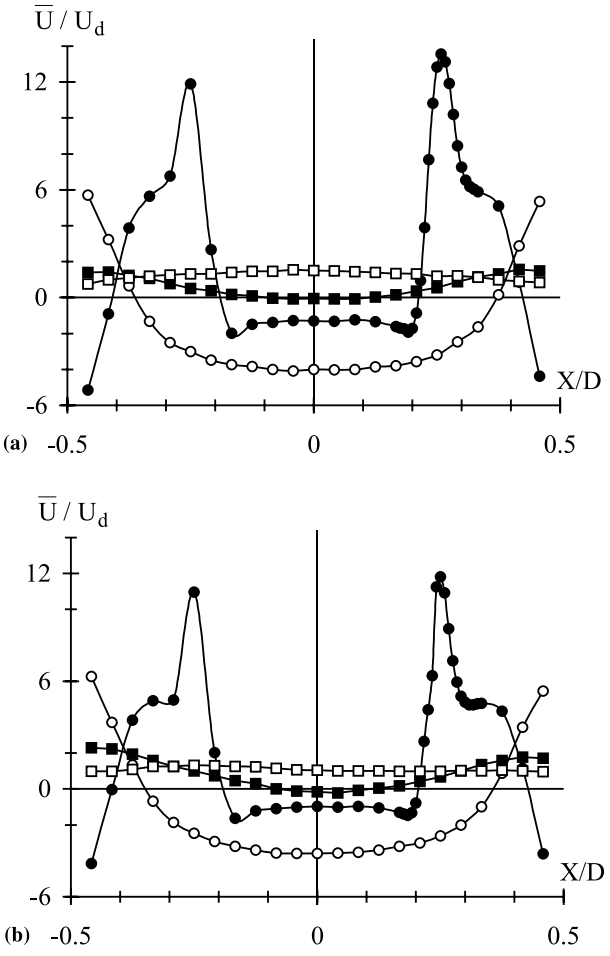

Fig. 2. Profiles of the mean axial velocities scaled by $U_d = 5$ m/s versus X/D, •: $Z/D = 0.17$; ○: $Z/D = 0.58$; ■: $Z/D = 1.21$; □: $Z/D = 2.17$. (a) Without swirl; (b) with swirl.

In the right part of Fig. 2 ($X > 0$), the experimental grid mesh is refined in order to capture more accurately velocity gradients.

4.1.2. With swirl

Fig. 2(b) shows the profiles of the axial mean velocity when the flow rig is fitted with the swirl generator. The same trends are observed as in the case without swirl. There are nevertheless some differences: the recirculation zone behind the valve is somewhat more extended in the longitudinal direction, the magnitude of the maximum velocity in the jet is smaller due to the presence of a tangential velocity. It is also observed that the jet width is smaller probably because of the flow separation from the valve or its seat.

4.2. Effect of non-homogeneity

4.2.1. Symmetry of the correlation coefficient curve

It is well known that in the case of homogeneous turbulence, the correlation coefficient curve is symmetric when displacing the moving probe on one side ($r > 0$) or on the other ($r < 0$). One should wonder whether the non-homogeneity of the investigated flow would be reflected on this property or not. Fig. 3(a) reveals that the departure from symmetry remains small far away from the jet centreline.

It should be noted that the measured correlation coefficient at zero separation is less than unity as indicated by earlier works (Eriksson and Karlsson, 1995; Trimis and Melling, 1995; Belmabrouk and Michard, 1998). This bias is essentially due to the finite size of the probe volume and has been investigated theoretically in Belmabrouk (2001). Its magnitude depends on the ratio of the probe volume length to turbulence length scales. On the presented curves (Fig. 3(a)), far away from the jet, integral length scale is equal to 5.6 mm and Taylor length scale is about 2 mm. Hence, $R(0)$ is very close to unity and the bias induced by the finite length of the probe volume length is very minor. However, in the jet, integral length scale is equal to 1.4 mm and Taylor length scale is about 0.7 mm. Consequently, the value of $R(0)$ is less than unity ($R(0) \approx 0.93$) and the bias due to spatial resolution is important for very small separations.

To quantify more exactly the degree of symmetry, we present in Fig. 3(b) the quantities:

$$\Lambda^{+}(r,\boldsymbol{x}) = \int_0^r R_{ii}^{(j)}(r',\boldsymbol{x})\,\mathrm{d}r' \quad \text{if } r > 0,$$
$$\Lambda^{-}(|r|,\boldsymbol{x}) = \int_r^0 R_{ii}^{(j)}(r',\boldsymbol{x})\,\mathrm{d}r' \quad \text{if } r < 0. \tag{3}$$

These parameters indicate the contribution of each range of probe distance to the integral scale. They tend to $L_{ii}^{(j)}$ for large separations. When the fixed probe is not situated in the jet

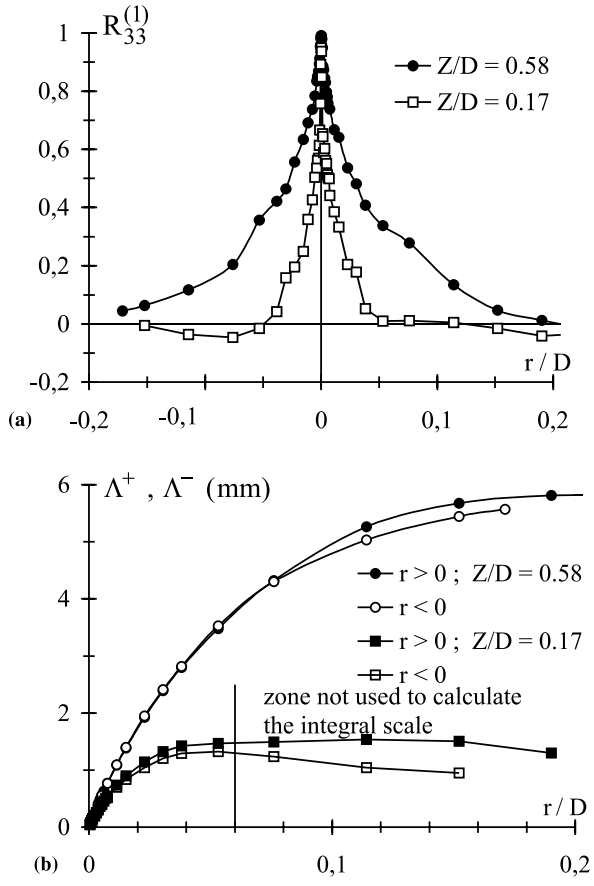

Fig. 3. Verification of the symmetry of the correlation curve far away from the jet flow ($Z/D = 0.58$, $X/D = 0.125$) and in the jet flow ($Z/D = 0.17$, $X/D = 0.25$). (a) Correlation curve; (b) contribution to integral scale (Eq. (3)).

flow, it is clear that up to a separation of about 10 mm both the branches are superimposed. The difference of 4% observed on the values of the integral scale is of the same order of magnitude as the experimental error, therefore it may not be only assigned to the non-symmetry. In the jet zone, the asymmetry of the curve becomes prominent (Fig. 3(a)) and the two branches of the correlation curve behave differently. However, the portion of the curve where non-symmetry is accentuated is not used to calculate the integral scale and the difference between the two values of the integral scale is less than 10% (Fig. 3(b)).

In brief, the displacement of the moving point along different directions leads to similar results and the difference on the integral scale is significant only at the frontier zone. Nevertheless, this mixing zone is strongly perturbed and turbulence may be out of equilibrium and the definition of integral scale may be devoid of physical meaning.

4.2.2. Comparison of two definitions of the correlation coefficient

In the upper section ($Z/D = 0.17$) where the non-homogeneity is strongly marked, depending on the position of the fixed point, the moving point either stays always in the same zone or crosses many zones of the flow. This leads to two definitions of the correlation coefficient and the corresponding integral scales. First, the correlation coefficient is obtained by normalising the correlation product by the RMS turbulent velocities of the fixed and moving points like in Eq. (1). For the second definition, normalisation is achieved only by the RMS value of the fixed point:

$$R_{ii}^{(j)}(r,\boldsymbol{x}) = \frac{\overline{u_i(\boldsymbol{x},t)\,u_i(\boldsymbol{x}+r\boldsymbol{e}_j,t)}}{\overline{u_i^2(\boldsymbol{x},t)}}. \tag{4}$$

Fig. 4 illustrates the profiles of the integral scales $L_{33}^{(1)}$ measured in the section $Z/D = 0.17$ by using either Eq. (1) or (4). The agreement of the two curves shows that the two approaches provide nearly the same results except in the shear layer between the recirculation and jet zones. Behind the central valve, the RMS value of the axial turbulent velocity is quasi-uniform in a given section, and for this reason the two definitions agree very well. In the jet, $\overline{u_3^2}$ changes with the position of the moving point, but the integral scale is small, so there is no appreciable variation of the $\overline{u_3^2}$ over the separation range related to the portion of the correlation curve used to determine the integral scale. However, at the frontier between the jet and the recirculation zone, the spatial gradients of $\overline{u_3^2}$ modify $L_{33}^{(1)}$. These results are in accordance with Fig. 3 that deals differently with the effect of non-homogeneity.

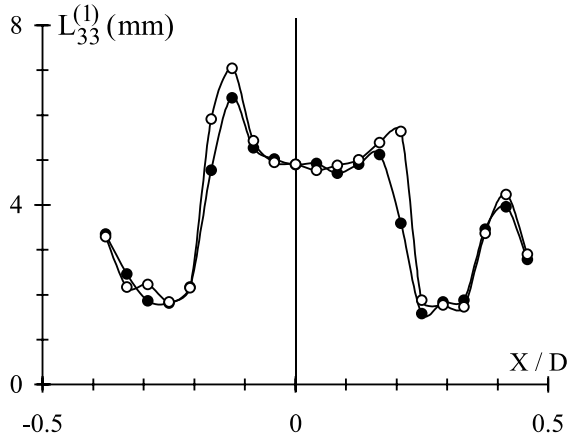

Fig. 4. Influence of the non-homogeneity on the integral length scale ($Z/D = 0.17$, $L_v = 10$ mm, with swirl) •: Eq. (1); ○: Eq. (4).

4.3. Profiles of integral length scale

Figs. 5(a) and (b) present the radial profiles of the integral scale $L_{33}^{(1)}$ measured with or without swirl in the sections $Z/D = 0.17$, 0.58 and 1.21. It appears that these profiles are weakly affected by the presence of the swirl. In the section $Z/D = 0.17$, it is observed that the integral scale is nearly uniform in the recirculating zone behind the valve. It decreases in the valve jet zone and increases again in the vicinity of the cylinder wall (secondary vortex). This behaviour is expected and may be qualitatively interpreted from the velocity profiles. The increase of the scale in the shear layer is attributed to the mean velocity gradient. The profiles measured in the sections $Z/D = 0.58$ and 1.21 show clearly the homogenisation process at a given section except for the external region of the flow. Near the side wall, the integral scale $L_{33}^{(1)}$ exhibits a decrease in the section $Z/D = 0.58$. In contrast, in the section $Z/D = 1.21$, a high increase of the integral scale appears for distances from the wall less than $0.17D$. This behaviour is observed in both investigated cases.

Fig. 6 presents some correlation coefficient curves measured, in the swirling case, in the section $Z/D = 1.21$ and for several locations of the fixed probe volume. For $X/D \leqslant 0.33$, the curves differ slightly, therefore the corresponding integral scales are very close to each other as observed in Fig. 5(b). From $X/D > 0.33$, the correlation coefficient related to a given

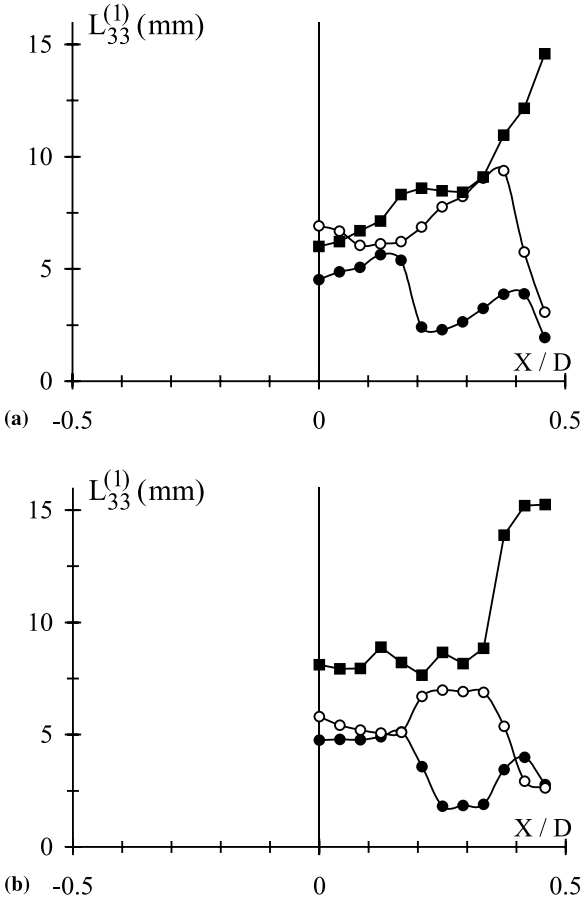

Fig. 5. Profiles of the integral scale $L_{33}^{(1)}$. (a) With swirl, (b) without swirl, •: $Z/D = 0.17$, ○: $Z/D = 0.58$, ■: $Z/D = 1.21$.

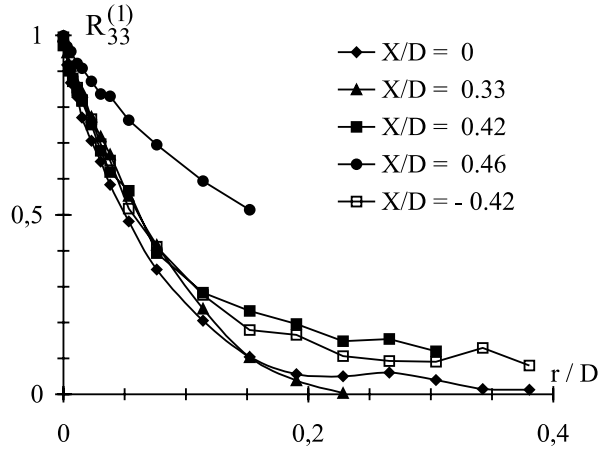

Fig. 6. Curves of the correlation coefficient versus r/D at the section $Z/D = 1.21$ for several positions of the fixed probe volume and for two diametrically opposed points (with swirl).

separation r increases when increasing the distance X. It results in a greater increase of the integral scale observed for the points near the wall. It should be noted that the integration of each correlation curve is performed up to the final measured point which is located very close to the wall and extrapolation of the curves seems meaningless.

To verify that the increase of $L_{33}^{(1)}$ in the external region is neither related to the local characteristics of the flow nor to an artefact of the experimental data processing, the correlation curve $R_{33}^{(1)}(r)$ is measured at two diametrically opposed points located at a distance $X/D = 0.08$ from the wall (Fig. 6). The superposition of the two curves shows that the increase of $L_{33}^{(1)}$ is due to some physical mechanism rather than the experimental set-up. To support this result, measurements are carried out in the section $Z/D = 2.08$, i.e. in a region far from the cylinder head where there is no recirculating flow. In the swirling case, the value of $L_{33}^{(1)}$ related to the fixed point at $X/D = 0.38$ is 16.6 mm whereas the value measured on the axis in only 8.6 mm.

4.4. Parametric study of the integral scale

The effect of the valve lift on the integral length scale $L_{33}^{(1)}$ has also been investigated (Fig. 7). It is observed that this effect is different depending on whether the fixed point is situated in the recirculation zone or the jet. Indeed, in the recirculation zone, the integral scale proves to be independent of the valve lift. The size of the large turbulent eddies in this region is very likely imposed by the valve head diameter and is not sensitive to the evolution of the intake jet. On the contrary, in the jet zone, integral scale exhibits a strong dependence on valve lift. It can be seen in Fig. 7 that $L_{33}^{(1)}$ first increases with increasing valve lift, then reaches a maximum and finally decreases. This non-monotonous evolution is certainly due to the flow separation from the valve head or seat at high lifts, inducing a throttling of the jet in the valve passage (Heywood, 1987).

4.5. Effect of swirl on different kinds of integral length scales

4.5.1. Comparison of the integral length scales with and without swirl

Fig. 8 exhibits different kinds of integral length scales measured on the cylinder axis, i.e. in the zone where the turbulence is almost homogeneous. This figure indicates that integral scales $L_{33}^{(1)}$ for the cases with and without swirl are very close, in other words the swirl has no important effect on this kind of integral scale. However, the presence of swirl modifies the integral scale $L_{22}^{(3)}$ in the region far away from the cylinder head. In the strongly perturbed zone that is near the cylinder head, the influence of swirl is not distinctly revealed. This may be explained by the fact that in this zone, the mixing and different mechanisms of turbulent kinetic energy production have a contribution as important as the production related to rotation.

The increase of $L_{22}^{(3)}$ in the case with swirl may be due to two mechanisms:

- the effect of solid body rotation as in homogeneous turbulence (Jacquin, 1987),
- the effect of swirl precession that induces large coherent structures (large fluctuations of the tangential velocity component w or u_2 in the axial direction 3).

4.5.2. Effect of solid body rotation

The effect of solid body rotation on turbulence scales is described by a homogeneous effect and a non-homogeneous effect. The homogeneous effect is usually characterised by the Rossby number:

$$Ro = \frac{u'}{2\Omega L} = \frac{1/2\Omega}{L/u'}, \tag{5}$$

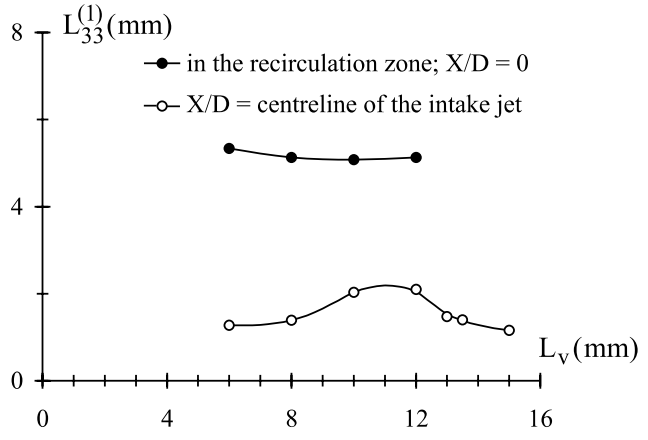

Fig. 7. Evolution of the integral length scale $L_{33}^{(1)}$ versus the valve lift L_v. ($Z/D = 0.17$, with swirl).

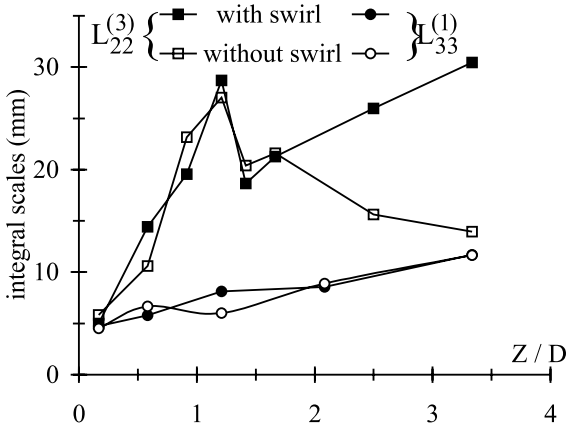

Fig. 8. Effect of swirl on the integral length scales $L_{33}^{(1)}$ or $L_{22}^{(3)}$. ($X/D = 0$, $L_v = 10$ mm).

where u' is the RMS value of the turbulent velocity, L is the integral scale and Ω is the rotation rate. The second form of the previous relation allows to interpret the Rossby number as being the ratio between a characteristic time of rotation and a characteristic time of turbulence. The homogeneous rotation effects appear only for Ro smaller than 1. The non-homogeneous rotation effect is characterised by the Eckman number:

$$E = \frac{v}{2\Omega L^2}$$

or by the parameter

$$J = \frac{Ro}{\sqrt{E}}.$$

When J decreases, the flow is marked more by the non-homogeneous effect.

Table 2 presents the order of magnitude of the Rossby number at the section $Z/D = 3.33$. The Rossby number, Ro, is of order 0.1. That is the customary order for which homogeneous effect of rotation appears. Therefore, non-homogeneity provoked by the walls has a small effect on the integral length scale. The behaviour of integral scales far away from the cylinder head agrees with the measurements and the predictions obtained by Jacquin (1987) in a turbulent swirling flow. Therefore, it may be believed that there is a specific effect of the rotation on turbulence scales. To confirm this assertion, one has to perform a spectral analysis and to filter the spectral modes related to the swirl centre precession.

4.5.3. Spectral density of the tangential turbulent velocity

It is well known that swirl provokes a large-scale, unsteady motion (Arcoumanis et al., 1987). Fig. 9 presents the profiles of the RMS of the turbulent tangential velocity w' measured at the sections $Z/D = 1.67$, 2.5 and 3.33; the swirl generator is excluded or included. When there is no swirl, the profiles of w' are uniform far away from the cylinder head but near the cylinder head ($Z/D = 1.67$), an increase of w' is observed. This increase is probably produced by instability motions occurring in the vicinity of the end of the recirculation zone. On the contrary, in the swirling case, it is clear that all profiles of w' exhibit a hump around the cylinder axis. The increase of w' in the central part is potentially assigned to the swirl centre precession, in other words to variations which are not turbulent but which are rather induced by instability motions.

To characterise more precisely the swirl centre precession and frequency of this periodic motion, we plot in Figs. 10 and 11 the spectral density of the tangential turbulent velocity measured on the cylinder axis at several sections. When the swirl generator is excluded (Fig. 10), a well-marked peak is observed at the section $Z/D = 1.67$. This peak is related to the increase of w' observed in (Fig. 9) for $Z/D = 1.67$. This peak diminishes downstream and the spectrum at the section $Z/D = 3.33$ approaches that of turbulence in spectral equilibrium. However, when the swirl generator is included (Fig. 11), the peak intensity increases downstream of the recirculation

Table 2
Order of magnitude of the Rossby number at the section $Z/D = 3.33$

Velocity component	Displacement	Integral scale	*Ro*	*J*
Axial	Axial	$L_{33}^{(3)}$	0.13	24
Axial	Radial	$L_{33}^{(1)}$	0.13	24
Tangential	Axial	$L_{22}^{(3)}$	0.07	35
Tangential	Radial	$L_{22}^{(1)}$	0.12	35

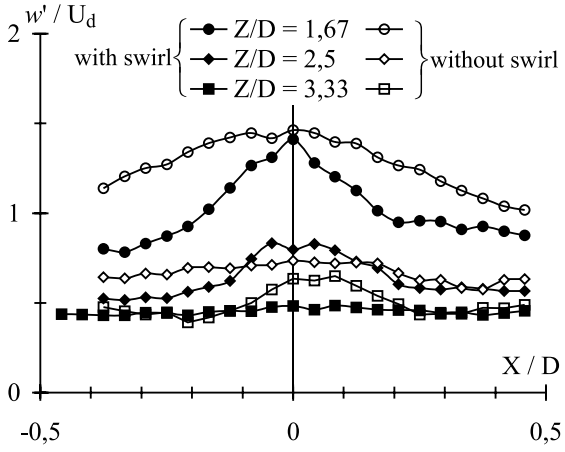

Fig. 9. Profiles of the tangential RMS velocity w' scaled by U_d.

zone. The peak in the swirling case is then due to large-scale motions.

The low-frequency periodic tangential motions lead to an overestimation of the correlation coefficient $R_{22}^{(3)}$ and the integral scale $L_{22}^{(3)}$. One should wonder if the experimental trends of integral scales (Fig. 8) are mainly due to the effect of solid body rotation on homogeneous turbulence or the presence of large-scale coherent structures. To quantify the contribution of periodic tangential motions to the correlation coefficient and to the integral scale $L_{22}^{(3)}$, temporal signals of the tangential fluctuating velocity at the fixed and moving probes are filtered by removing the spectral modes related to the peak, they are then correlated again to obtain the so-called filtered $R_{22}^{(3)}$. Since the data rate used to perform these measurements is very high

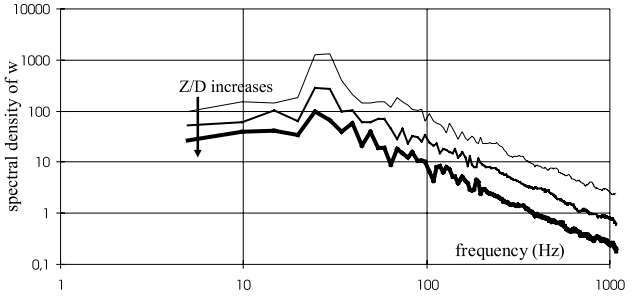

Fig. 10. Frequency analysis of the instantaneous tangential velocity ($Z/D = 1.67$ or 2.5 or 3.33, $X/D = 0$, without swirl).

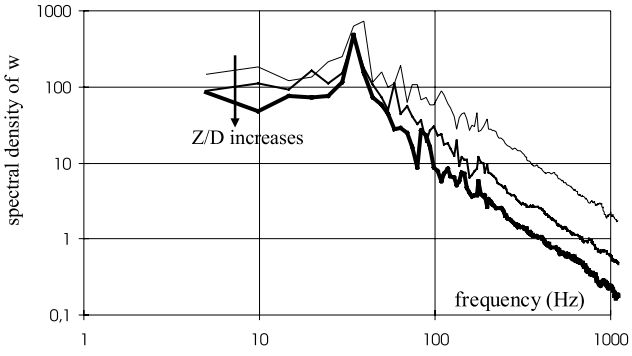

Fig. 11. Frequency analysis of the instantaneous tangential velocity ($Z/D = 1.67$ or 2.5 or 3.33, $X/D = 0$, with swirl).

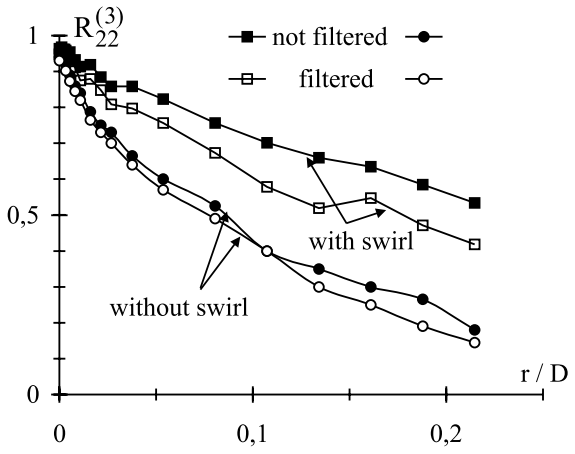

Fig. 12. Effect of frequency filtering on the correlation coefficient (•: not filtered, ○: filtered).

(more than 20 kHz), it is expected that no significant artefacts are introduced in the data processing to generate the spectra from randomly sampled data (van Maanen and Oldenziel, 1998).

Fig. 12 shows the correlation coefficient $R_{22}^{(3)}$ obtained before and after the temporal signal filtering. Although this filtering procedure leads to a decrease of the correlation level especially in the swirling case, it does not modify the qualitative trends related to the effect of rotation. The signal processing by spectral filtering confirms that the increase of the integral scale observed in the swirling case by using an ensemble average is actually due to the effect of the swirling motion on the turbulent field.

5. Conclusion

The mean and RMS velocities and the integral length scales have been measured by laser Doppler velocimetry to investigate a simplified flow simulating the intake stroke of a reciprocating engine. Depending on the kind of integral scale ($L_{22}^{(3)}$ or $L_{33}^{(1)}$), the swirl may or may not have an important effect on this scale. The spectral analysis confirms this result and demonstrates the presence of a large-scale instability motion due to the swirl-centre precession. The effect of the swirl is greater on the integral scale $L_{22}^{(3)}$ than on the RMS of the tangential velocity.

Acknowledgements

Thanks are due to Nathalie Grosjean and to Djamal Safsaf for the technical assistance. This paper comes within the framework of a collaborative project 'action intégrée du comité mixte franco-tunisien de coopération universitaire' (CMCU n° 97 F 11 12). The authors gratefully acknowledge this financial support.

References

Arcoumanis, C., Hadjiapostolou, A., Whitelaw, J.H., 1987. Swirl center precession in engine flows. Society of Automotive Engineers, Technical Paper 870370.

Belmabrouk, H., 2001. Accuracy of Taylor length scale measurements by two-point laser Doppler velocimetry. Flow Measurement and Instrumentation 12, 9–16.

Belmabrouk, H., 1992. Mesure des échelles de longueur par vélocimétrie Doppler laser en deux points. PhD thesis, Ecole Centrale de Lyon, France.

Belmabrouk, H., Lance, M., Grosjean, N., Michard, M., 1991. Turbulence length scale measurements by two-point laser Doppler anemometry in a steady flow. Society of Automotive Engineers, Technical Paper 910474.

Belmabrouk, H., Michard, M., 1998. Taylor length scale measurements by laser Doppler velocimetry. Exp. Fluids 25, 69–76.

Eriksson, J.G., Karlsson, R.I., 1995. An investigation of the spatial resolution requirements for two-point correlation measurements using LDV. Exp. Fluids 18, 393–396.

Heywood, J.B., 1987. Fluid motion within the cylinder of internal combustion engines. J. Fluids Eng. 109 (3), 3–35.

Jacquin, L., 1987. Etude théorique et expérimentale de la turbulence homogène en rotation. PhD thesis, Université Claude Bernard, Lyon, France.

Lance, M., Belmabrouk, H., Gervais, Y., Grosjean, N., Michard, M., 1991. Aérodynamique interne d'un moteur axisymétrique entraîné. In: La Combustion Dans les Moteurs d'Automobile, Technip, Paris, pp. 133–150.

Trimis, D., Melling, A., 1995. Improved laser Doppler anemometry techniques for two-point turbulent flow correlations. Meas. Sci. Tenhol. 6, 663–673.

van Maanen, H.R.E., Oldenziel, A., 1998. Estimation of turbulence power spectra from randomly sampled data by curve-fit to the autocorrelation function applied to laser-Doppler anemometry. Meas. Sci. Technol. 9, 458–467.